CellPress

Neuron
Article

Target-Independent EphrinA/EphA-Mediated Axon-Axon Repulsion as a Novel Element in Retinocollicular Mapping

Philipp Suetterlin[1] and Uwe Drescher[1,*]
[1]MRC Centre for Developmental Neurobiology, New Hunt's House, Guy's Campus, Kings College London, London SE1 1UL, UK
*Correspondence: uwe.drescher@kcl.ac.uk
http://dx.doi.org/10.1016/j.neuron.2014.09.023

SUMMARY

EphrinAs and EphAs play critical roles during topographic map formation in the retinocollicular projection; however, their complex expression patterns in both the retina and superior colliculus (SC) have made it difficult to uncover their precise mechanisms of action. We demonstrate here that growth cones of temporal axons collapse when contacting nasal axons in vitro, and removing ephrinAs from axonal membranes by PI-PLC treatment abolishes this response. In conditional knockout mice, temporal axons display no major targeting defects when ephrinA5 is removed only from the SC, but substantial mapping defects were observed when ephrinA5 expression was removed from both the SC and from the retina, with temporal axons invading the target areas of nasal axons. Together, these data indicate that ephrinA5 drives repellent interactions between temporal and nasal axons within the SC, and demonstrates for the first time that target-independent mechanisms play an essential role in retinocollicular map formation in vivo.

INTRODUCTION

The retinotectal/collicular projection describes the axonal connection between the retina and the tectum (fish/frog/chick), or its mammalian homolog, the superior colliculus (SC), and represents a key model system for studying the development of topographic maps. Here neighborhood relationships are preserved such that cells neighboring in one field are connected to cells neighboring in another field, facilitating a faithful transfer of positionally organized information from one area to another. In the retinotectal/collicular projection, the temporal retina is connected to the rostral tectum/SC and the nasal retina to the caudal tectum/SC, while the dorsal and ventral retina are connected to the lateral and medial tectum/SC, respectively.

Members of the EphA/ephrinA family, which were cloned in the 1990s (Cheng et al., 1995; Drescher et al., 1995), turned out to be prominently involved in controlling the development of this projection (Feldheim and O'Leary, 2010; Huberman et al., 2008; Triplett and Feldheim, 2012). Strikingly, the expression patterns of several EphA and ephrinA family members combine to give rise to counter gradients in both the retina and the SC (Figure 1). Fitting well with the chemoaffinity hypothesis formulated by Sperry (1963), temporal retinal ganglion cell (RGC) axons with high EphA receptor expression map to the rostral SC, which expresses low amounts of ephrinAs, while nasal RGC axons with low EphA receptor expression project to the caudal SC with high ephrinA expression.

According to the prevailing concept, temporal axons develop termination zones (TZs) in the rostral SC since their formation in the caudal SC is suppressed by high concentrations of repellent ephrinA ligands. In a knockout (KO) of the three ephrinAs, which are expressed in the retinocollicular projection (ephrinA2, ephrinA3, and ephrinA5), temporal axons form ectopic TZs (eTZs) more caudally. However, the phenotypes are less prominent or completely absent when only a subset of these three ephrinAs are deleted (Pfeiffenberger et al., 2006) indicating a correlation between the expression levels of ephrinAs and the severity of the targeting defects.

The mechanisms underlying the mapping of nasal axons to the caudal SC remain poorly understood. Nasal axons also express substantial amounts of EphA receptors (albeit at lower levels than temporal axons; Reber et al., 2004) and therefore should also be repelled from growing into the caudal SC. However, retinal axon terminals have the tendency to fill their entire target areas uniformly, possibly to maximize their synaptic coverage (Schmidt, 1978). As a result of this, nasal axons are thought to fill the available space in the caudal SC because they are less sensitive to the ephrinA gradient than temporal axons. In ephrinA triple KO (TKO) mice, as described above, a subset of temporal axons form eTZs more caudally, and as a consequence of this, they might "push" the branching of a portion of nasal axons to more rostral positions. Indeed, nasal axons do form eTZs rostral to the main TZ in the ephrinA TKO (Pfeiffenberger et al., 2006).

Seminal genetic experiments using EphA knock-in and KO approaches have provided strong support for the idea that relative, but not absolute, levels of EphA receptor signaling are important for normal map development. These studies suggested that retinal axons can somehow "compare" the strength of EphA signaling to that of neighboring axons and shift to more rostral or caudal positions correspondingly. The authors concluded that this relative signaling mechanism was based on target-dependent axon-axon interactions (Brown et al., 2000; Reber et al., 2004).

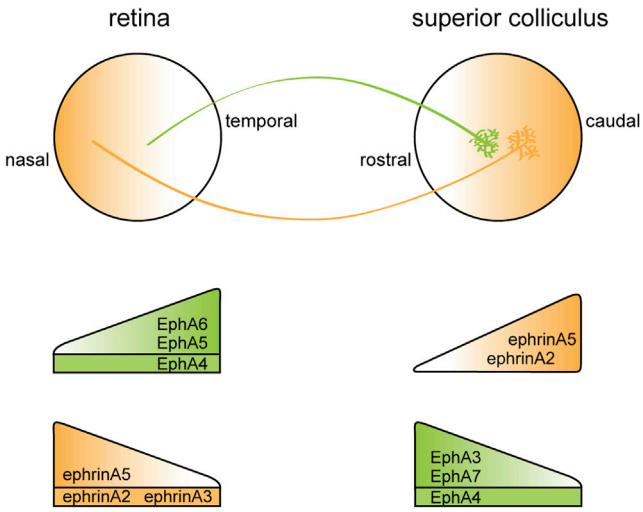

Figure 1. The Retinotectal/Collicular Projection

Projection pattern of temporal and nasal RGC axons in the retinocollicular projection combined with the expression patterns of EphAs and ephrinAs in both the retina and the SC. EphrinA5 is expressed in a gradient in both the retina and the superior colliculus (SC), while ephrinA2 is expressed in a gradient in the SC, but shows no obvious differential expression in the RGC layer (Pfeiffenberger et al., 2006) (Figure S1). EphrinA3 is expressed in the RGC layer in no obvious gradient, while its expression in the SC is hardly detectable (Pfeiffenberger et al., 2006) (Figure S1). Moreover, multiple EphA receptors are expressed in gradients or uniformly in the retina and the tectum/SC (McLaughlin and O'Leary, 2005).

In the scheme, the orange gradients in retina and SC represent the expression of ephrinA5 only. For clarity, the gradients of the other ephrinAs as well as the EphAs are omitted.

Servomechanism models propose that a single ephrinA gradient can have both positive and negative effects that serve to guide RGC axons to their correct topographic position, meaning that the ephrinA gradient in the SC might be attractant at low concentrations and repellent at high concentrations (Hansen et al., 2004; Honda, 2003).

Since ephrinAs are expressed also in the retina, and EphAs also in the SC (Figure 1), a number of additional axon-target as well as axon-axon interactions between EphA- and ephrinA-expressing cells are possible. This is further enhanced by the capacity of EphAs and ephrinAs to signal bidirectionally, a defining feature of the Eph family (Davy and Soriano, 2005; Klein, 2009). This means that EphA receptors can function also as ligands, and ephrinAs also as receptors.

The dual-gradient model combines bidirectional signaling and axon-target interactions. According to this model, a second gradient system—formed by ephrinAs with a receptor function expressed on retinal axons (nasal > temporal) and EphAs with a ligand function expressed in the SC (rostral > caudal)—also contributes to the mapping process (Figure 1; Suetterlin et al., 2012). This model is supported by a number of EphA KO and knock-in approaches (Carreres et al., 2011; Lim et al., 2008; Rashid et al., 2005; Yoo et al., 2011) as well as in vitro experiments (Gebhardt et al., 2012; Lim et al., 2008; Marler et al., 2010; Rashid et al., 2005).

In addition, the expression patterns of EphAs/ephrinAs in the retinocollicular projection strongly predict axon-axon interactions. Thus, repellent interactions between predominantly ephrinA-expressing nasal axons that target the caudal SC, and predominantly EphA-expressing temporal axons that target the rostral SC, are expected to be an important element of topographic mapping. For example, this type of interaction would prevent an intermixing of TZs of temporal and nasal retinal axons in the central part of the SC, but may well be involved in topographic mapping processes throughout the entire SC.

Classic in vitro experiments by F. Bonhoeffer and colleagues performed in the 1980s make a strong case for the potential importance of repellent axon-axon interactions for topographic mapping in the visual system (Bonhoeffer and Huf, 1980, 1985; Raper and Grunewald, 1990). These experiments demonstrated that when given the choice, temporal axons avoid nasal, but not temporal, axons, while nasal axons did not appear to have an obvious preference for either. These findings uncovered for the first time the principle of repellent axon-axon interactions for RGCs, although the significance for topographic mapping in vivo could only be anticipated at the time.

However, more recent computational modeling has highlighted axon-axon interactions as an important, if not necessary, component for retinocollicular map formation (Gebhardt et al., 2012; Yates et al., 2004). It is thought that the collicular ephrinA gradient may be enhanced or sharpened by the contribution of axonal ephrinAs on ingrowing nasal axons themselves (Figure 1). During the initial ingrowth phase (i.e., in the absence of axonal branching) their contribution to total ephrinA levels might be negligible; however, extensive branching/arborization of nasal axons in the caudal SC during later stages of map development might dramatically increase the amount of axon-derived ephrinAs in the caudal SC and contribute to topographic specificity.

Here we have combined in vitro approaches and the analysis of ephrinA5 conditional KO mice to investigate the significance of axon-axon interactions for the development of the retinocollicular projection and to study the function of ephrinA5 on retinal axons versus its function in the SC.

RESULTS

In Vitro Analysis of Axon-Axon Interactions

In vitro experiments from the 1980s showed that temporal axons are repelled upon contact with nasal axons in the chick (Bonhoeffer and Huf, 1980, 1985; Raper and Grunewald, 1990). However, the molecular nature of the axonal repellent expressed on nasal axons could not be identified back then (e.g., guidance cues including ephrinAs were not cloned at that time). We have readdressed this question here and have studied the encounter of temporal with nasal axons (T→N) as well as nasal-temporal (N→T), temporal-temporal (T→T), and nasal-nasal (N→N) interactions in the presence (or absence) of PI-PLC, an enzyme which specifically cleaves glycosyl-phosphatidyl-inositol (GPI)-anchored proteins including ephrinAs from the membrane (Hornberger et al., 1999).

We found that without PI-PLC treatment, temporal axons showed a strong growth cone collapse response after contact with nasal axons, while the collapse rates for the other types of interactions were much weaker (Figure 2). Intriguingly, treatment with PI-PLC strongly reduced the growth cone collapse rate of

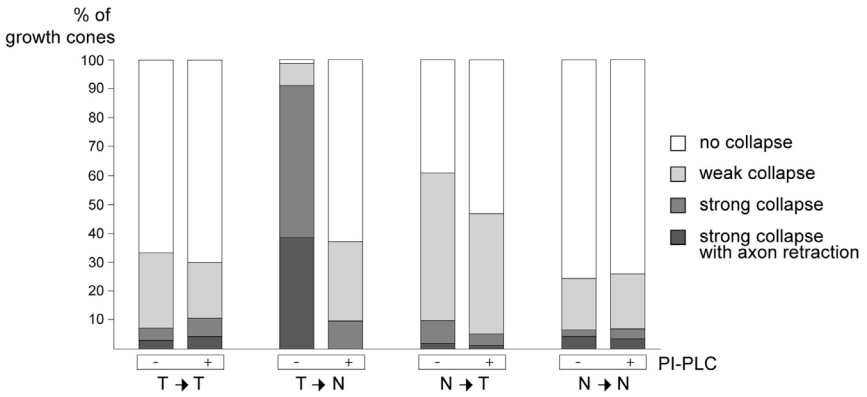

Figure 2. PI-PLC Treatment Abolishes Growth Cone Collapse of Temporal RGC Axons after Contact with Nasal Axons

Quantification of growth cone collapse rate for the interaction of temporal (T) and nasal (N) chick RGC axons, derived from a > 3 hr time-lapse analysis in the presence (+) or absence (−) of PI-PLC. The data show the sum of three independent experiments for each condition (with and without 0.3 U/ml PI-PLC added at least 5 hr before start of the analysis). For all four possible interactions, at least ten encounters were analyzed in each single experiment. Details of the experimental setup and the scoring system to classify axon-axon interactions (no, weak, or strong growth cone collapse, or strong growth cone collapse with retraction) are given in Experimental Procedures. Examples for the different classes of growth cone collapse are shown in Movies S1–S4.

The data show a strong growth cone collapse of temporal axons when contacting nasal axons, which is abolished after treatment with PI-PLC. A statistical analysis using a three-way chi-square test shows significant differences for the category of interactions without PI-PLC treatment ($p < 0.001$), and no significant differences for the interactions with PI-PLC treatment ($p = 0.058$).

T→N interactions to a level similar to those observed for the other three interactions (Figure 2). While PI-PLC treatment affects all GPI-anchored proteins, the most parsimonious explanation seems to be that the removal of ephrinAs from nasal axons in these cultures essentially reduces growth cone collapse to baseline levels.

Our in vitro data therefore confirm F. Bonhoeffer's early in vitro findings and offer a good molecular candidate, i.e., ephrinAs, for the growth cone collapse-inducing activity of nasal axons.

Description of EphrinA5 Conditional KO Mice

To analyze the role of ephrinAs on RGC axons in vivo, we used ephrinA5 conditional "KO-first" mice (Skarnes et al., 2011) (Figure S2A available online), which we obtained from the International Knockout Mouse Consortium (IKMC) and the European Conditional Mouse Mutagenesis (EUCOMM) project. In these mice, loxP sites flank the second exon of the *ephrinA5* gene, which contains most of the coding region of ephrinA5, while the first exon contains only the first 20 amino acids (aa) of the mature protein, which comprises in total 228 aa. Thus, a conditional, Cre-mediated excision of exon 2 abolishes the synthesis of a functional ephrinA5 transcript (Figure S2C). For the widely published full KO of ephrinA5, a comparable approach was taken, that is, deletion of exon 2 by homologous recombination (Feldheim et al., 1998; Frisén et al., 1998).

In addition, these KO-first mice harbor a splice acceptor-IRES-lacZ cassette, flanked by frt sites, in the intron preceding exon 2 (Figure S2A) (Skarnes et al., 2011), which abolishes the normal splicing from exon 1 to exon 2. Since we were interested here in analyzing retinocollicular mapping after a conditional inactivation of ephrinA5 in either the retina, the SC, or both (Figure S2C), we first removed this SA-IRES-lacZ cassette by breeding them with mice expressing flp recombinase ubiquitously (http://www.jax.org) thereby restoring the normal splicing/expression of the *ephrinA5* gene while retaining the loxP sites flanking exon 2 (Figure S2B).

In order to abolish expression of ephrinA5 in the retina, a mouse line was chosen in which Cre is expressed under the control of the rx promoter (rx:cre) (Swindell et al., 2006), and for inactivation of ephrinA5 in the SC, the En1$^{cre/+}$ line, in which Cre is expressed from the endogenous engrailed-1 promoter (Basson et al., 2008). Both lines have been extensively characterized (Basson et al., 2008; Swindell et al., 2006). Expression of rx starts at E8.5 in the entire prospective optic vesicle; accordingly Cre will be expressed in all RGCs. While there is additional expression in the entire forebrain (see also Ackman et al., 2012; Pinter and Hindges, 2010), expression of ephrinA5 in the SC is unaffected. The en1$^{cre/+}$ line contains cre as a knock-in into the en-1 locus, thus is heterozygous for *engrailed-1*, but shows no phenotype (Basson et al., 2008). Engrailed-1 is expressed specifically in the midbrain/hindbrain from very early in development. Although being expressed in a caudal > rostral gradient in the SC, expression of Cre is strong enough to achieve recombination throughout the SC (Basson et al., 2008).

We have reconfirmed the expression pattern of Cre by crossing these mice to a reporter line in which a stop-floxed YFP cassette has been integrated into the ubiquitously active rosa26 locus (*R26*-stop-EYFP; http://www.jax.org). We then analyzed YFP expression on retinal cross sections as well as parasagittal brain sections containing the SC (Figures 3A–3D).

Figures 3A and 3B show representative parasagittal sections through the brains of offspring from an en1:cre; R26-YFP cross and a rx:cre; R26-YFP cross, respectively. Evidently, en1:cre drives strong and highly localized YFP expression in the superior and inferior colliculi as well as in the cerebellum, whereas those areas are devoid of YFP signal in the rx:cre; R26-YFP cross.

Conversely, analysis of retinal sections derived from rx:cre; R26-YFP mice revealed widespread YFP expression throughout the retina, but no signal above background for en1:cre; *R26*-stop-EYFP mice (data not shown). As observed by others (Cai et al., 2010), rx:cre apparently fails to induce recombination in a small subset of retinal domains (Figure 3C).

Furthermore, to measure Cre recombinase activity at a more global level, we extracted mRNA from P0 whole retinae or the central third of the SC from control pups (ephrinA5$^{fl/fl}$; "wt" in Figure 3E), pups with a retinal KO (rx:cre; ephrinA5$^{fl/fl}$), or a collicular

KO (en1:cre; ephrinA5$^{fl/fl}$). RT-PCR was used to determine the tissue-specific expression levels of ephrinA5. In the collicular KO ("en1"), ephrinA5 expression in the SC was almost completely abolished (Figure 3F), while the retinal ephrinA5 expression was unchanged compared to wild-type controls (Figure 3E). For the retinal KO ("rx"), ephrinA5 expression levels in the SC appeared unchanged (Figure 3F), while the retinal ephrinA5 expression was dramatically reduced, although some detectable expression remained (Figure 3E). This is in agreement with previous reports where the rx:cre driver line was used to excise other floxed genes in the retina (Dhande et al., 2012).

Moreover, we analyzed these mice by mRNA in situ hybridization experiments for ephrinA expression. The gradient expression of ephrinA5 in the retina (Figures 3G–3K, 3M, and 3N) was almost completely abolished in the retinal KO (Figures 3L, 3O, and 3P) and apparently does not affect the retinal expression of ephrinA2 and ephrinA3 (Figure S1). Conversely, in the collicular KO, ephrinA5 expression was completely abolished (Figures 3Q and 3R) with no apparent change in the expression profiles of ephrinA2 and ephrinA3 (Figure S1).

Projection Pattern of Retinal Axons from the Temporocentral Retina

Following their nonspecific ingrowth into the SC, temporal and nasal axons branch extensively at topographically specific locations, and this process eventually leads to the formation of densely arborized TZs. Accordingly, temporal axons develop axonal arborizations preferentially in the rostral SC, and nasal axons in the caudal SC (Figure 1). Since ephrinAs are predominantly expressed on nasal axons, we hypothesized that the developing branches/arbors in the caudal SC would increasingly contribute to the overall ephrinA gradient that prevents temporal axons from branching there. Consequently, deletion of retinal ephrinA5 should lead to targeting defects of temporal axons. EphrinA5 conditional KO mice are particularly suitable for these analyses since ephrinA5 is the only ephrinA expressed in an obvious nasal > temporal gradient in the retina, while ephrinA2 and ephrinA3 appear more uniformly distributed (Figures 1, 3, and S1) (Pfeiffenberger et al., 2006).

To investigate this hypothesis in detail, we analyzed two axonal populations which project to adjacent territories in the central SC, that is, axons from the centrotemporal retina and axons from the centronasal retina, which therefore might preferentially show targeting defects due to disturbed repellent axon-axon interactions. We have analyzed wild-type mice and mice with a KO of ephrinA5 in the retina (rx:cre; ephrinA5$^{fl/fl}$), in the SC (en1:cre; ephrinA5$^{fl/fl}$), or in both the retina and the SC (en1:cre; rx:cre; ephrinA5$^{fl/fl}$).

In wild-type mice, axons from the temporocentral retina (t-axons) formed a clear and focused TZ in the rostrocentral area of the SC (Figure 4A, arrow; n = 14). A parasagittal section shows the ingrowth of retinal axons from the rostral pole, and TZ formation in deeper layers of the SC (Figure 4B, arrow). In mice with a deletion of ephrinA5 only in the colliculus (en-1:cre; ephrinA5^{fl,fl} mice), t-axons showed only very minor targeting defects (Figures 4C and 4D), that is, weak eTZs were observed caudal to the main TZ (Figures 4C and 4D, arrow). Similarly, weak eTZs as shown in Figure 4C were observed in all mice with only a collicular ephrinA5 deletion (100% penetrance; n = 13). In some cases we observed single axons meandering in the SC (Figure 4C, arrow heads). This means that abolishing only the collicular expression of ephrinA5 has very little effect on the mapping of t-axons.

Furthermore, a deletion of ephrinA5 only from retinal axons (retinal KO; rx:cre; ephrinA5$^{fl/fl}$) did not lead to the formation of eTZ caudal to the main TZ (Figures 4E and 4F).

However, when ephrinA5 was removed from both SC and retina (en1:cre; rx:cre; ephrinA5$^{fl/fl}$) (Figures 4G and 4H), we observed strong eTZs in the caudal SC (100% penetrance; n = 8).

A quantitative analysis of the relative strength of the eTZ showed that the eTZs in the retinal+collicular KO were about three times stronger than those in the collicular KO alone (Figure 4I). A further quantification demonstrated that for both collicular and retinal+collicular KOs, axonal populations from the same topographic area in the retina were analyzed (Figure 4J; see Experimental Procedures). This showed that the differences in the strength of the eTZs were not due to the labeling of retinal axons from different positions along the N-T axis (see below; Figure S3). Interestingly, the eTZs were formed at the same topographic position in the collicular versus the retinal+collicular KO (Figure 4J).

Taken together, these data show that topographic mapping of t-axons is largely intact when only the collicular expression or only the retinal expression of ephrinA5 is abolished. However, when ephrinA5 is removed from both nasal retinal axons and collicular cells, the topographic mapping of t-axons is substantially disturbed; t-axons now form robust eTZs more caudally, in a territory that clearly is already the target area of nasal axons (Figures 4G, 4H, 4J, and S3). In summary, removal of ephrinA5 from the SC and retinal axons leads to an intermingling of the TZs of temporal and nasal axons and a disruption of topographic order (Figures 7 and S3).

Thus, as long as ephrinA5 is expressed on nasal retinal axons, temporal axons form almost normal TZs in their regular target area, and only after the removal of the axonal expression of ephrinA5, temporal axons show robust topographic targeting defects. As described above, these data fit very well with in vitro experiments showing that temporal axons are repelled by nasal axons (Bonhoeffer and Huf, 1980, 1985) (see also section "In Vitro Analysis of Axon-Axon Interactions"; Figure 2). In the Discussion we further detail why the phenotype of caudal eTZs in particular indicates a disruption of axon-axon, but not axon-target, interactions (and see below).

In addition to the formation of eTZs of temporal axons in a territory normally occupied by nasal eTZs, we observed—albeit at low frequency—eTZs rostral to the main TZ in the retinal and in the retinal+collicular KO, but not in the collicular KO (Figures 4E–4H; n = 15, 40% penetrance for the retinal; n = 8, 25% penetrance for the retinal+collicular KO). These observations are consistent with a role of ephrinA reverse signaling in defining the rostral limits of TZs as predicted by the dual-gradient model (see Discussion) (Carvalho et al., 2006; Hornberger et al., 1999; Kao and Kania, 2011; Marquardt et al., 2005; Rashid et al., 2005).

Targeting Errors of Axons from the Centronasal Retina

Next, we analyzed the projection pattern of axons from the centronasal part of the retina (n-axons; Figure 5), which in the

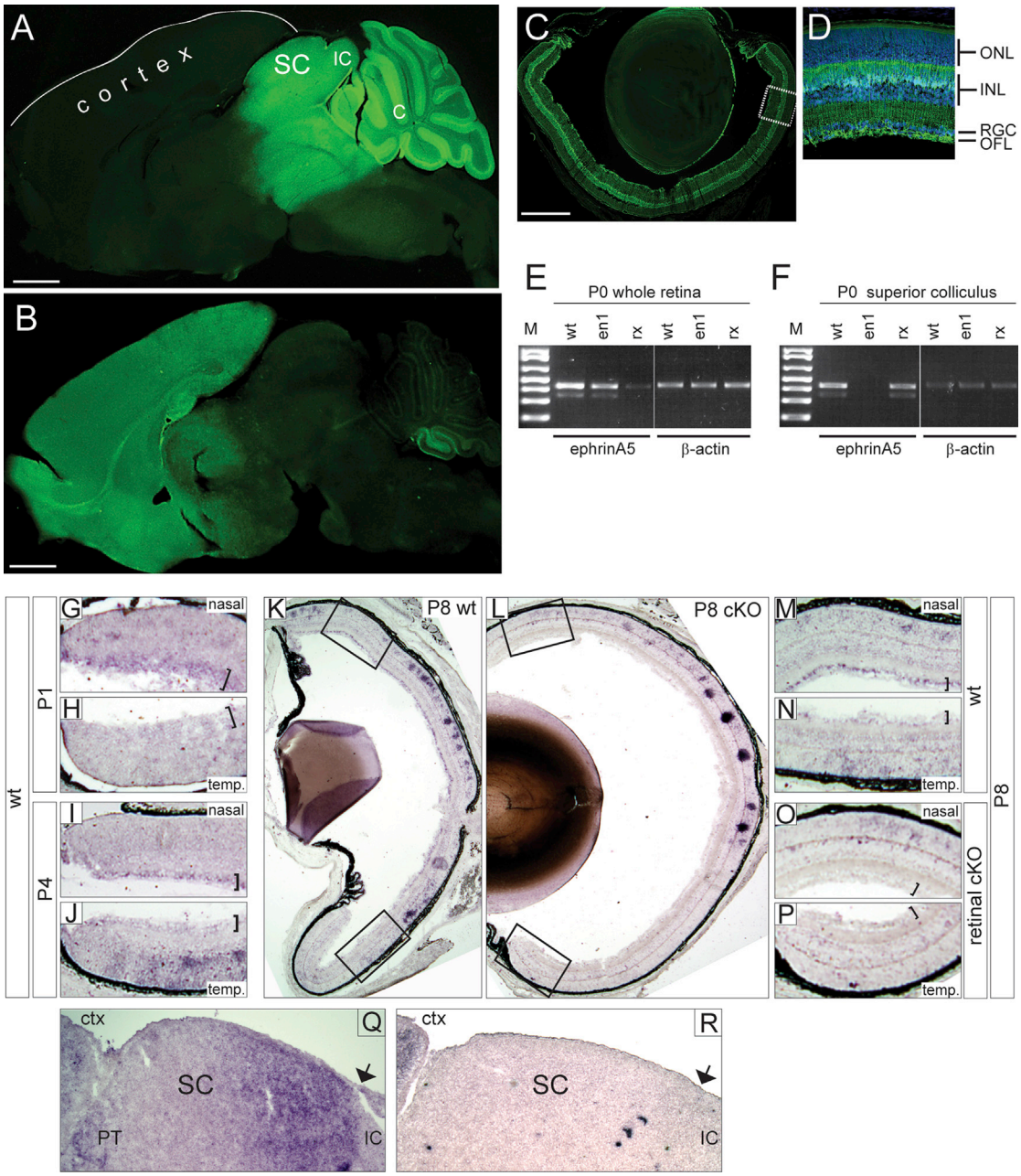

Figure 3. Characterization of the Conditional EphrinA5 Line

(A–D) Verification of the tissue-specific expression of Cre recombinase in the cre-driver lines used. Cre lines were crossed with *R26*-stop-EYFP reporter mice (see Experimental Procedures). Cre expression will excise the stop cassette allowing expression of YFP, thereby visualizing all cells in which Cre has been active.

(A) Parasagittal brain section from a cross between *R26*-stop-EYFP and en-1:cre mice at P12. The SC, the inferior colliculus (IC), the cerebellum (C), and the cortex are indicated. YFP is strongly expressed in the SC, IC, and cerebellum, but not in the cortex.

(B) Parasagittal brain section from a cross between *R26*-stop-EYFP and rx:cre mice at P12. Expression of YFP is mostly confined to the forebrain and excludes the SC.

(C) Section of the retina of *R26*-stop-EYFP x rx:cre mice at P12. YFP is expressed throughout the retina.

(D) Enlargement of the area boxed in (C), to highlight expression of YFP in the optic fiber layer containing the axons of RGCs.

(E and F) RT-PCR analysis of ephrinA5 expression using cDNA prepared from RNA that was isolated from P0 retinae and SCs of en-1:cre; ephrinA5$^{fl/fl}$ (en-1) or rx:cre; ephrinA5$^{fl/fl}$ (rx) or wild-type (wt) mice. Agarose gel analysis shows an almost complete abolishment of ephrinA5 expression in the retina (E), but not the SC (F), of rx:cre; ephrinA5$^{fl/fl}$ mice, and a complete abolishment of expression of ephrinA5 in the SC (F), but not the retina (E), of en1:cre; ephrinA5$^{fl/fl}$ mice. RT-PCR analysis performed in parallel using β-actin-specific primers shows that comparable amounts of cDNA were used (see Experimental Procedures).

ONL, outer nuclear layer; INL, inner nuclear layer; OFL, optic fiber layer. Scale bars in (B), 1 mm; scale bars in (C), 500 μm.

(legend continued on next page)

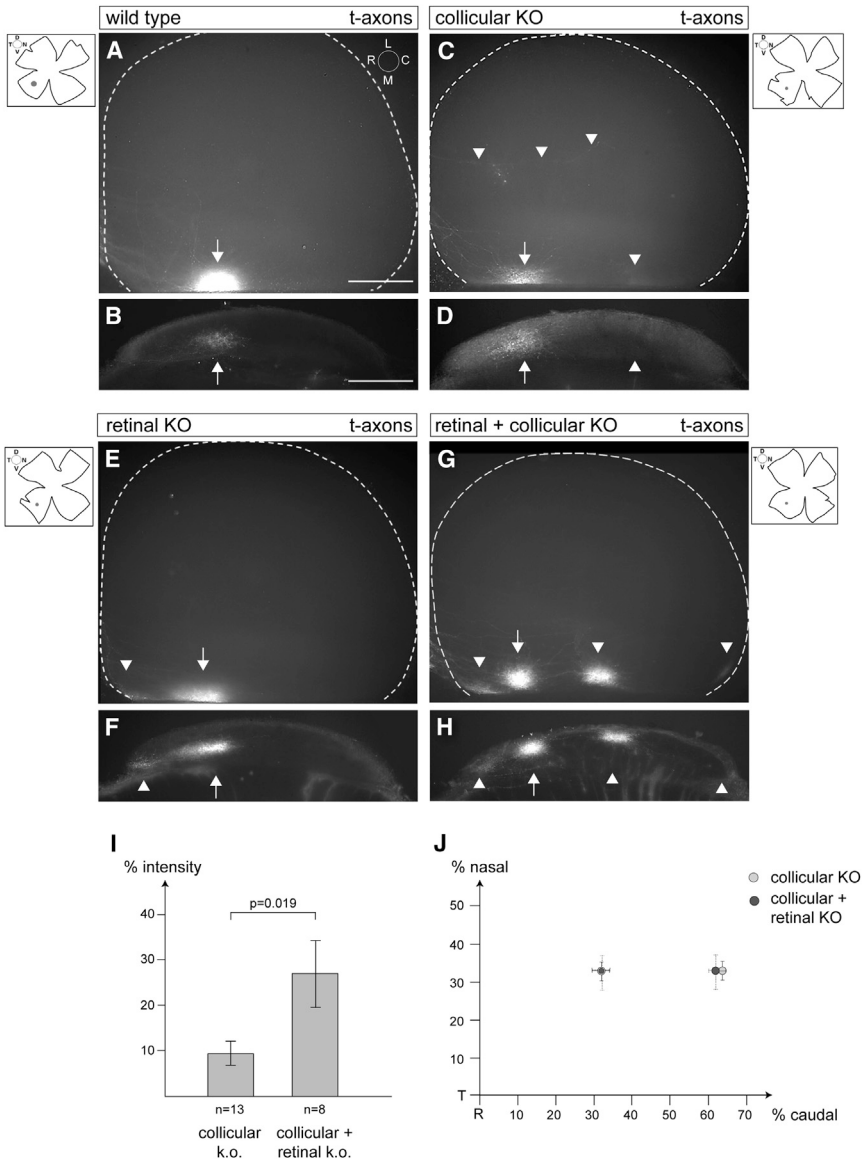

Figure 4. Projection Pattern of t-Axons in Wild-Type and EphrinA5 cKOs

DiI was focally injected at P8/P9, and fluorescence microscopy of SC whole mounts was carried out 1 day later. The injection site of DiI is indicated in drawings of the corresponding flat-mounted retina shown in a box adjacent to the whole mounts. SC whole mounts are shown (A, C, E, and G), with representative parasagittal sections below (B, D, F, and H).

(A and B) Whole mount (A) and corresponding parasagittal section (B) showing the projection pattern of t-axons in wild-type mice. The main TZ is indicated by an arrow.

(C and D) Projection pattern of t-axons in the collicular KO. A weak eTZ (arrowhead) is formed caudal to the main TZ (arrow). Additional arrowheads delineate a single overshooting axon.

(E and F) Projection pattern in the retinal KO. t-axons form a weak eTZ (arrowhead) rostral to the main TZ (arrow). A parasagittal section indicates that this eTZ is located within the SC. Penetrance of the rostral eTZ is 40% (n = 15).

(G and H) Projection pattern in the retinal+collicular KO. eTZs are formed caudal (arrowhead) and rostral (arrowhead) to the main TZ (arrow).

(I) Quantification of the intensity of the caudal eTZs formed in the collicular (C and D) and retinal+collicular (G and H) KOs. The relative intensity of the eTZs are given (eTZ and main TZ add up to 100%). The eTZ in the retinal+collicular KO is about three times stronger than the one in the collicular KO. The number of projections analyzed is given below the bars (see Experimental Procedures for further details; two-tailed Student's t test; p = 0.019).

(J) Analysis of the position of the main TZ and the caudal eTZ relative to the retinal DiI injection site show no statistically significant differences between collicular and retinal+collicular KO (using two-tailed Student's t test). SEM for the retinal+collicular KO is indicated by dotted lines.

All SC whole mounts are oriented as indicated representatively in (A), with rostral to the left and lateral to the top. The SC is outlined by a dotted line. Orientation of the retinal flat mount is indicated in the drawings with temporal to the left and dorsal to the top. The number of projections analyzed for each genotype and retinal population as well as the penetrance of phenotypes are detailed in the Results section. Error bars represent SEM. Figure S3 gives a summary of the projection patterns. Scale bar in (A) and (B), 500 μm. L, lateral; m, medial; r, rostral; c, caudal, as well as for the retinal flat mount with d, dorsal; v, ventral; t, temporal; n, nasal.

wild-type project to the centrocaudal SC (Figures 5A and 5B). Here we observed in mice with a collicular deletion of ephrinA5 (Figures 5C and 5D) a substantially stronger phenotype than that of t-axons, with the formation of a number of TZs widely dispersed over the central SC (n = 4, 100% penetrance). This phenotype was not overtly enhanced in mice with a deletion of ephrinA5 in both colliculus and retina (Figures 5E and 5F; n = 4, 100% penetrance). Thus, for both the collicular and the retinal+collicular KO, we observed up to four TZs, with two of them always having a strong appearance, while the additional

(G–R) Analysis of ephrinA5 expression by in situ hybridization analysis.

(G–L) EphrinA5 is expressed in the RGC layer in nasal, but not temporal, retina at postnatal day 1 (P1) (G and H), and P4 (I and J). At P8, there is strong ephrinA5 expression in the RGC layer of the nasal retina in wild-type (K), but not retinal KO (L), mice.

(M and N) Enlargement of boxed areas in (K) showing strong ephrinA5 expression in P8 nasal, but not in temporal, retina.

(O and P) Enlargement of boxed areas in (L) showing absence of ephrinA5 expression in nasal as well as in temporal retina.

(Q and R) EphrinA5 is expressed in a caudal > rostral gradient in the SC in wild-type mice (Q), but expression is completely abolished in the collicular KO (R). PT, pretectum.

Brackets in (G)–(J) and (M)–(P) indicate the RGC layer.

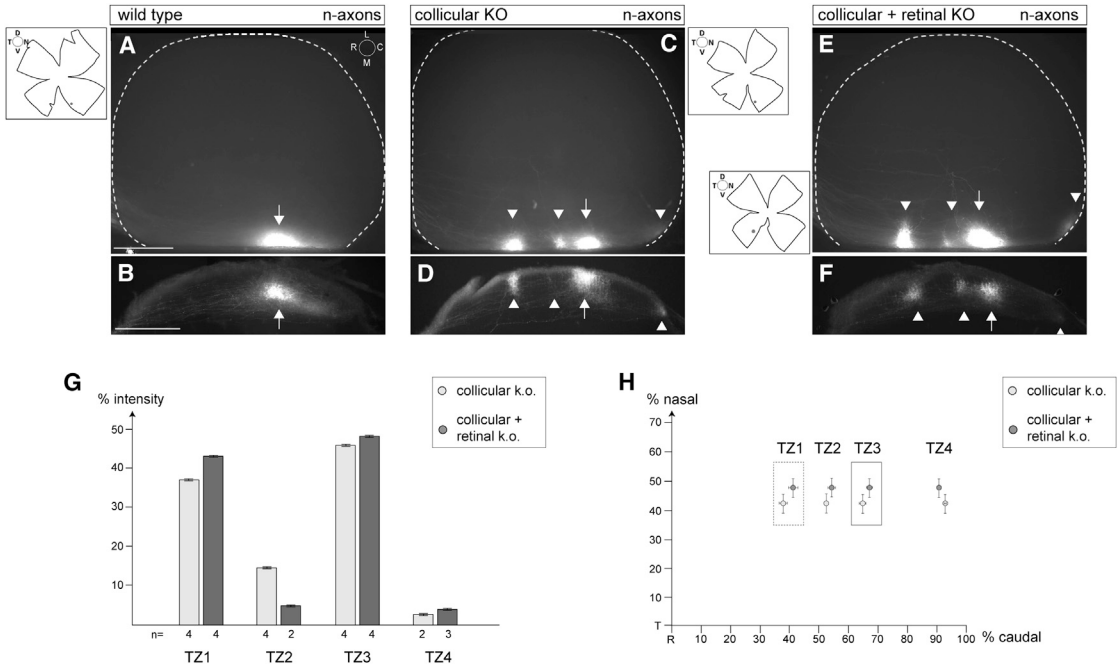

Figure 5. Projection Pattern of n-Axons in Wild-Type and EphrinA5 cKOs

DiI was focally injected at P8/P9, and fluorescence microscopy of SC whole mounts was carried out 1 day later. The injection site of DiI is indicated in drawings of the corresponding flat-mounted retina shown in a box adjacent to the whole mounts. SC whole mounts are shown (A, C, and E), with representative parasagittal sections below (B, D, and F).

(A and B) Whole mount (A) and corresponding parasagittal section (B) showing projection patterns of n-axons in wild-type mice. The main TZ is indicated by an arrow.

(C and D) Typical projection pattern of n-axons in the collicular KO. The main TZ (named TZ3 in G and H) is marked by an arrow. Additional TZs are formed rostrally and weakly also caudally (arrowheads). A quantification of intensity and location of the TZs is given in (G) and (H).

(E and F) Projection pattern in the retinal+collicular KO. The main TZ is marked by an arrow. Additional TZs are formed rostrally and caudally (arrowheads). Their quantification is shown in (G) and (H).

(G) Quantification of TZ intensity in the collicular and retinal+collicular KOs. The TZs (C)–(F) are labeled from rostral to caudal with the most rostral one named TZ1. Here TZ4 shows the least strong penetrance and shows also the weakest intensity (Frisén et al., 1998) and was not included in the quantification for technical reasons. Intensities of TZ1–TZ3 are given in percent (sum of all three TZs add up to 100%). The number of TZs is given below the bars; the two strongest ones (TZ1 and TZ3) are seen in all four cases, while TZ2 was observed in all four projections with a collicular KO, and in two out of four cases in the retinal+collicular KO.

(H) Analysis of the topographic position of the TZs and the retinal DiI injection sites shows no statistically significant differences between collicular and retinal+collicular KO (two-tailed Student's t test; retina, $p = 0.25$; TZ1, $p = 0.14$; TZ3, $p = 0.20$).

Error bars represent SEM. Scale bars in (A) and (B), 500 μm. For further details and abbreviations see Figure 4 and Figure 6 legends. A summary scheme of the projection pattern is shown in Figure S3.

TZs were much weaker (n = 4, penetrance 100%; Figure 5G). Comparison with wild-type and analysis of the retinal location of the DiI injection sites suggested that the strongest TZ was the topographically most appropriate (TZ3; Figure 5H). The second-strongest TZ was located rostral to the main TZ (TZ1; Figure 5H). The combination of relative TZ strength and TZ topography suggests that TZ1 is a rostrally shifted eTZ, and TZ3 the topographically most appropriate main TZ. The intensity of the TZs and eTZs of n-axons showed only subtle differences between the collicular and the retinal+collicular KO, which did not reach statistical significance (Figure 5G).

The main eTZ formed by n-axons (in the collicular and retinal+collicular KO) is located clearly in the rostral half of the SC (Figures 5H and S3) and thus intermingles with eTZs of temporal axons. However, the targeting defects of n-axons do not involve abolished repellent axon-axon interactions since the collicular phenotype of n-axons was not enhanced after removal of ephrinA5 from retinal axons (retinal+collicular KO). Therefore, the sheer deletion of the collicular ephrinA5 expression causes this rostral shift of n-axon targeting.

Moreover, we did observe very weak eTZs at the very caudal end of the SC in both the collicular and retinal+collicular ephrinA5 KOs (Figures 5C–5F, arrowhead; TZ4 in Figure 5H). However, only a small fraction of nasal axons behaved in this way, and it clearly did not represent the main phenotype observed for n-axons.

Targeting Errors of Nasal Axons

To better understand the behavior of n-axons, we turned our attention to the targeting behavior of axons from the very nasal periphery in the various ephrinA5 KOs. In wild-type mice, axons from the nasal periphery (nn-axons) project to the caudal pole of the SC (Figure 6A; n = 24). In the collicular KO (en1:cre; ephrinA5$^{fl/fl}$) we observed robust eTZs in more central areas of

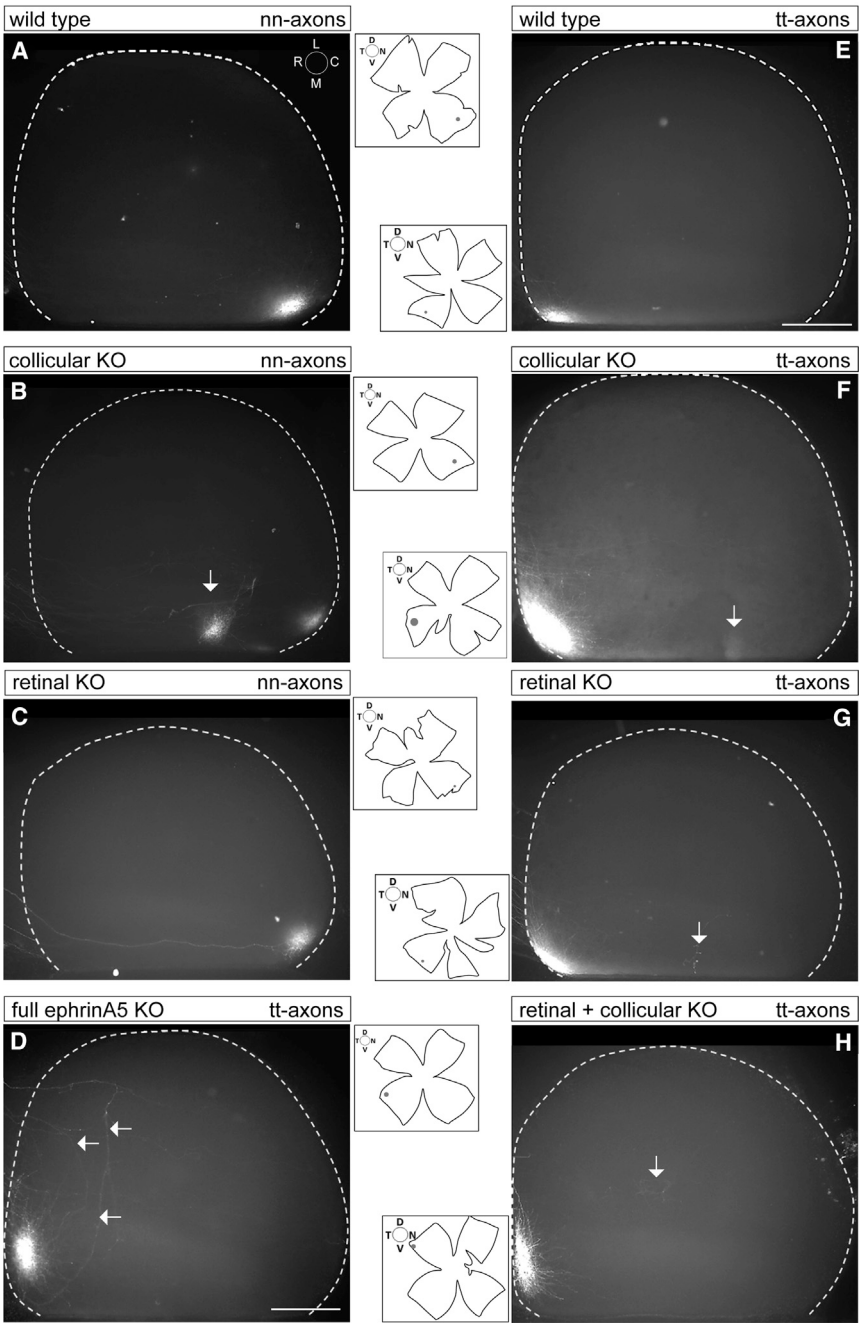

Figure 6. Projection Pattern of tt- and nn-Axons in Wild-Type and EphrinA5 cKO Mice

DiI was focally injected at P8/P9, and fluorescence microscopy of SC whole mounts was carried out 1 day later. The injection site of DiI is indicated in drawings of the corresponding flat-mounted retina shown in a box adjacent to the whole mounts.

(A–C) Analysis of nn-axon projection pattern after injection of DiI in the nasal periphery of the retina.

(D–H) Analysis of tt-axon projection pattern after injection of DiI in the temporal periphery of the retina.

(A) nn-axons in wild-type mice project to the nasal pole of the SC.

(B) In the collicular ephrinA5 KO, a substantial fraction of nn-axons project to more rostral positions of the SC forming here a tight eTZ (arrow).

(C) In a retinal ephrinA5 KO, nn-axons project to the caudal pole of the SC.

(D) In a full KO of ephrinA5, tt-axons project to the rostral pole, with very few axons mistargeting (aberrant axons indicated by arrows).

(E) In wild-type mice, tt-axons project to the rostral pole of the SC.

(F–H) In a KO of ephrinA5 in either the SC (F), the retina (G), or both (H), tt-axons show only very few targeting defects and form a major TZ in the rostral SC (aberrant axons and eTZs labeled by arrows). In (F), the SC from a particularly strong retinal DiI injection is shown to highlight the paucity of formation of eTZ in the collicular KO.

Further explanations are given in the Figure 4 and Figure 5 legends. A schematic summary of the projection patterns is given in Figure S3. Scale bar in (D) and (E), 500 μm.

the SC in all mice analyzed (Figure 6B; n = 17, penetrance 100%). Similar to the behavior of n-axons, again half of the nn-axons projected to more rostral positions. The strength of the targeting defect appears to be comparable to that of the ephrinA5 full KO described previously (Feldheim et al., 2000; Pfeiffenberger et al., 2006). In complete contrast to the collicular ephrinA5 KO, nn-axons essentially showed no phenotype in the retinal KO (Figure 6C; rx:cre; ephrinA5$^{fl/fl}$; n = 11).

Again, the rostral ectopic projection of nn-axons in the collicular KO cannot be explained on the basis of chemoaffinity (see above). It also cannot be explained on the basis of a non-cell-autonomous effect, such as a targeting defect that is secondary to the misrouting of temporal axons. Since targeting defects of t-axons are minimal in the collicular ephrinA5 KO and only lead to weak eTZs, which never reach the caudal extreme of the SC (see above), there is no reason to believe that they could cause the phenotype of nn-axons.

A good possibility to explain the collicular KO phenotype is that the flattening of the overall ephrinA gradient leaves nasal axons (nn- and n-axons) with insufficient targeting (positional) information to find their proper target zone, resulting in the formation of several TZs at various positions in the caudal SC.

Projection Pattern of Retinal Axons from the Temporal Periphery

Finally, we analyzed the targeting behavior of axons from the temporal periphery (tt-axons), which in wild-type mice form TZs at the very rostral pole (Figure 6E). In full agreement with data published by Pfeiffenberger and colleagues (Pfeiffenberger et al., 2006), we observed (somewhat surprisingly) only very

small or no targeting defects of tt-axons in either the collicular (Figure 6F; n = 15), the retinal (Figure 6G; n = 16), or the retinal+collicular ephrinA5 KO (Figure 6H; n = 3). However, in all three KO lines, we did occasionally observe individual axons that extended caudally past the main TZ. Sometimes these overshooting axons even formed coarse arbors (arrows in Figures 6G and 6H), and in some instances we detected very weak eTZs caudal to the main TZ, particularly in the collicular KO (Figure 6B, arrow; 53% penetrance; see Experimental Procedures).

To further substantiate this finding, we investigated the full KO of ephrinA5 (Figure 6D; n = 4) as well as the ephrinA2/ephrinA5 double KO (DKO; data not shown, n = 4). Again, we found only very weak targeting defects for tt-axons in the ephrinA5 full KO with a few axons overshooting caudally, but not forming discernible eTZs (arrows in Figure 6D). The phenotype was more pronounced in the ephrinA2/ephrinA5 DKO; the number of aberrantly projecting axons was markedly increased, but still failed to generate strong eTZs (data not shown). As indicated, these astonishing findings are in agreement with data from Pfeiffenberger et al. (2006). Here it was shown that only in the ephrinA2/ephrinA3/ephrinA5 TKO, and not in the ephrinA2/ephrinA5 DKO, axons from the temporal periphery show robust eTZs, which are confined to the rostral SC (Pfeiffenberger et al., 2006).

DISCUSSION

We show here that ephrinA5 expression on nasal axons is a key component of repellent axon-axon interactions, which prevents an intermingling of TZs of temporal and nasal axons during topographic mapping within the central SC. Our data provide in vivo evidence for a guidance principle during retinocollicular map development that is based on target-independent axon-axon interactions.

Repellent Axon-Axon Interactions between Temporal and Nasal Axons In Vitro and In Vivo

EphrinAs and EphAs show complex expression patterns in the retina and the SC during development of the retinocollicular projection, involving expression of ephrinAs preferentially on nasal axons and of EphAs preferentially on temporal axons. We have revisited in vitro experiments from the Bonhoeffer lab performed in the 1980s, which showed that temporal axons are repelled from contacting nasal axons (Bonhoeffer and Huf, 1980, 1985). We provide evidence that this behavior is due to ephrinA expression on nasal axons, since treatment with PI-PLC, which removes ephrinAs from axons, abolishes the repellent activity of nasal axons (Figure 2).

These in vitro data suggest that repellent axon-axon interactions driven by axonal ephrinAs/EphAs play a role during map formation in vivo. We hypothesized that branch formation of temporal axons in the caudal SC is suppressed not only by ephrinAs expressed by collicular cells, but also by ephrinAs located on nasal retinal axons (Raper and Grunewald, 1990), which extensively branch and arborize in the caudal SC during (ongoing) map development (Gebhardt et al., 2012; Yates et al., 2004). EphrinA5 in particular might be involved in this process, since it is the only ephrinA expressed in a strong nasal > temporal gradient, while ephrinA2 and ephrinA3 are expressed in no obvious gradients in the RGC layer (Figures 3 and S1).

Experimental evidence for the hypothesis that target-independent axon-axon interactions play a role in these mapping processes in vivo has been lacking so far, since this would require a selective removal of ephrinAs from either the retina or the SC.

Taking advantage of conditional ephrinA5 KO mice, we found that abolishing only the collicular expression of ephrinA5 (collicular KO) did not substantially affect the targeting of axons from the temporocentral retina (t-axons; Figure 4C). However, when ephrinA5 expression was also removed from retinal axons (that is, in a retinal+collicular KO), the targeting of t-axons was strongly disrupted, and these axons formed robust eTZs in the caudal SC, i.e., invaded the targeting area of nasal axons (Figures 4G, 7, and S3). This means that the expression of ephrinA5 on nasal axons (i.e., with an abolition of the collicular expression of ephrinA5) mostly prevents temporal axons from invading the caudal SC, and only if in addition ephrinA5 expression from nasal axons is removed, temporal axons invade the caudal SC. These data show that specific axon-axon interactions are involved in topographic mapping in the retinocollicular projection.

Alternative Explanations for this Phenotype?

Given the complexity of the expression patterns of ephrinAs and EphAs in the retina and SC, and considering their capacity for reverse and forward signaling, some alternative explanations to explain the targeting effects of t-axons appear possible, but, we believe, are less likely on close examination.

First and foremost, one could argue that the formation of caudal eTZs of temporal axons is a cell-autonomous effect and a direct consequence of changing ephrinA5 concentrations on t-axons themselves. The effects of altering axonal ephrinA concentrations were investigated in vitro and in vivo (Dütting et al., 1999; Hornberger et al., 1999). However, these studies suggest that the removal of ephrinAs from retinal axons should in fact have the opposite effect (i.e., rostral eTZs) from what is observed here (caudal eTZs). In particular, a decrease of ephrinAs on retinal axons led to an increase in their sensitivity toward external ephrinAs, while an increase in ephrinA expression on retinal axons was shown to lead to a decreased sensitivity toward external ephrinAs (Dütting et al., 1999; Hornberger et al., 1999). These changes in sensitivity have been linked to *cis* interactions of EphAs and ephrinAs on retinal axons (e.g., masking; Carvalho et al., 2006). As indicated above, applied to our data, a retinal KO of ephrinA5 should therefore lead to an increase in sensitivity to external ephrinAs, and as a consequence, t-axons should form eTZ rostrally since they would now be more strongly repelled by the caudal > rostral ephrinA gradient. However, as shown for the ephrinA5 retinal+collicular KO, the main eTZs are formed caudally. This argues indeed against a cell-autonomous effect for this particular mapping defect.

Second (or as an alternative view of the argument given above), ephrinAs might function on retinal axons as repellent receptors (Rashid et al., 2005; Suetterlin et al., 2012). However, again, a removal of ephrinAs would then be expected to shift

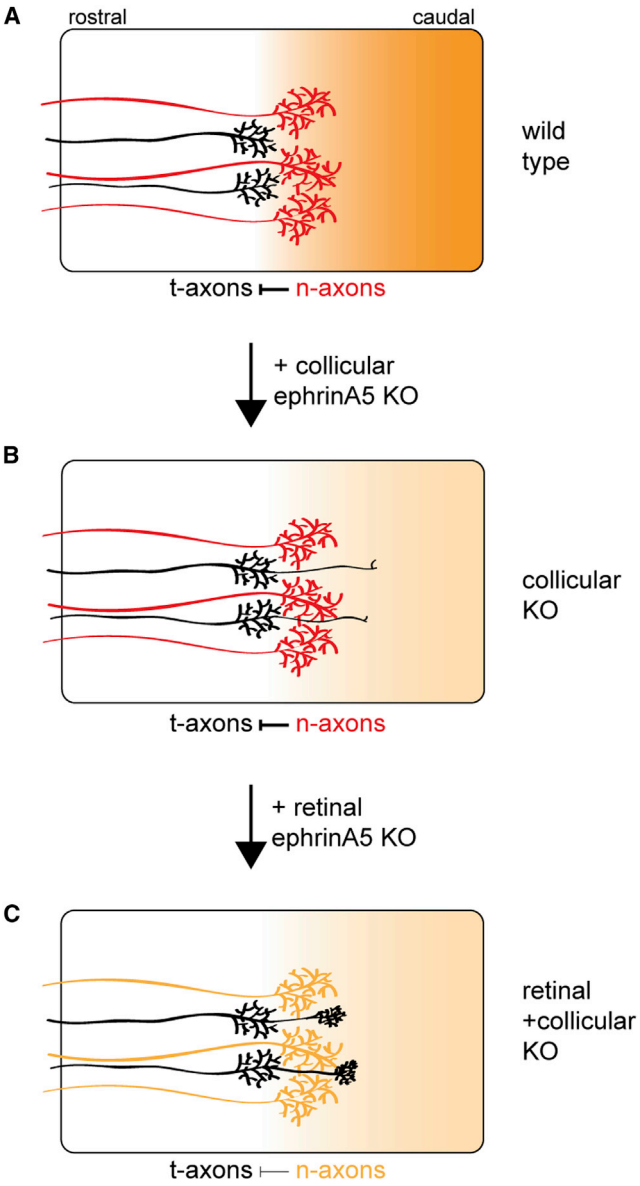

Figure 7. Target-Independent Axon-Axon Interactions Control Topographic Mapping of t-Axons

Our model to explain the caudal targeting defects of t-axons is based on a functional ephrinA gradient in the SC, which is made up of two components: ephrinAs expressed by collicular cells (caudal > rostral gradient, shown in deep orange) and an import of ephrinAs by nasal axons (red), which branch and form TZs in the caudal SC.

(A) In wild-type, t-axons (black) project to the rostrocentral SC, while n-axons project to the caudocentral SC. t-axons do not invade the caudal SC due to the expression of ephrinAs on nasal axons and on cells of the caudal SC.

(B) In the collicular ephrinA5 KO, the expression that is the repellent activity of ephrinAs in the caudal SC is reduced (indicated by a light orange gradient); however, t-axons are still repelled from invading the caudal SC by expression of ephrinAs on nasal axons (red).

(C) In the retinal+collicular ephrinA5 KO, the repellent activity of the caudal SC is further reduced since now ephrinA5 expression on nasal axons is also abolished (orange). The targeting of t-axons is strongly disrupted, and these axons now formed robust eTZs in the caudal part of the SC invading the territory of nasal axons.

eTZs to a more rostral position, since these axons would be less repelled from the rostral > caudal EphA gradient (as proposed by the dual-gradient model). In fact, besides the caudal eTZ (100% penetrance for the retinal+collicular KO), we observed with low penetrance (40% penetrance for the retinal KO) a small fraction of t-axons forming eTZs rostrally, which lends support to this view. The occasional appearance of eTZs rostral and caudal to the main TZ in the retinal+collicular KO indicates that t-axons are guided by multiple mechanisms, including a suppression of branching rostrally (possibly via a receptor function of ephrinAs) and a suppression of branching caudally (by the expression of ephrinAs on nasal axons and SC). Irrespective of the mechanisms by which the rostral eTZs are formed, the argument that the caudal eTZs are formed by disrupted axon-axon interactions remains valid.

Third, it also seems very unlikely that the phenotype of t-axons is a secondary effect caused by an interference with nasal axons that are misguided rostrally. If this were the case, the phenotype of t-axons should already be apparent in the collicular KO, where n-axons exhibit a phenotype indistinguishable from the retinal+collicular KO. This, however, is not what we observed.

Lastly, immunohistochemical approaches have shown that ephrinA5 expression on t-axons is rather low (Lim et al., 2008; Marcus et al., 1996), which makes it improbable, although not impossible, that a deletion of ephrinA5 from the retina directly affects t-axons. As argued above, an indirect effect—caused by a deletion on nasal axons which express ephrinA5 at much higher levels—appears more likely.

Taken together, it appears that the most likely explanation for the caudal overshooting of t-axons is the abolition of repellent axon-axon interactions with nasal axons in the retinal+collicular KO, which suggests that specific axon-axon interactions are indeed an element of topographic mapping in the retinocollicular projection.

The repellent axon-axon interactions have been demonstrated in vivo only for ventronasal and ventrotemporal axons, and not, for example, dorsonasal or dorsotemporal axons. However, our in vitro data did not show any differential sensitivities along the DV axis making it likely that this new mapping principle is relevant for all nasal and temporal axons.

Based on the analysis of solitary axons in the zebrafish retinotectal projection, Gosse et al. (2008) put forward the idea that axon-axon interactions are not required for topographic mapping; however, as the authors further specify, this argument holds true only for the distal part of TZs which mapped appropriately even in solitude, while the proximal end of their TZs was in fact significantly extended rostrally. While the authors argued for the existence of a second tectum-derived gradient necessary to restrict the proximal end of a TZ (Gosse et al., 2008), possibly repellent N→T axon-axon interactions might lead here to the same effect.

Our data indicate the importance of the axonal expression of ephrinA5 for the normal development of the retinocollicular map in the segregation of temporal and nasal axons, since t-axons can robustly invade the caudal SC only if ephrinA5 is removed from nasal axons. For clarity, in this scheme, the mistargeting of nasal axons as well as the formation of rostral eTZs of t-axons is not depicted (see Figure S3 for a summary of all targeting defects).

The Targeting Behavior of Peripheral Temporal Axons

We show here that peripheral temporal axons are largely unaffected by the deletion of ephrinA5 from the colliculus and/or retinal axons (Figures 6F–6H), or in the full ephrinA5 KO (Figure 6D), and even mostly map to their normal topographic position in the ephrinA2/ephrinA5 DKO (n = 4; data not shown). Our data for the DKO resemble those of Pfeiffenberger et al. (2006), who found robust targeting defects only if additionally ephrinA3 was deleted, i.e., in the TKO (Pfeiffenberger et al., 2006). These astonishing findings suggest that targeting of peripheral temporal axons might involve other and/or additional activities, for example, engrailed (Brunet et al., 2005; Wizenmann et al., 2009) (see also Willshaw et al., 2014). Furthermore, uniform expression of ephrinA3 in the retina and no detectable expression in the retinorecipient layers of the SC adds another layer of complexity to the mapping process, but highlights the importance of retinal ephrinA expression.

The Targeting Behavior of Nasal Axons

Retinal axons from the centronasal area of the retina (n-axons) are strongly affected in the collicular KO of ephrinA5, where they form prominent eTZs in rostral locations and also a weak eTZ at the very caudal pole of the SC (Figure 5C) (Frisén et al., 1998). This phenotype is not enhanced in mice with an additional retinal ephrinA5 KO (Figure 5E), demonstrating that the mapping of n-axons is predominantly controlled by collicular, and not (or to a much lesser extent) by retinal, ephrinA5. Given the severity of phenotypes, there is a good possibility that the mapping defects of centronasal axons involve interference from mistargeted peripheral nasal axons. Conversely, it is highly unlikely that their mapping defects are a secondary consequence of the comparably weak overshooting and eTZ formation of t-axons within the caudal SC (Figure 4C).

We think that the targeting defects of nasal axons in the collicular ephrinA5 KOs are most likely caused by a reduction in positional information linked to a flattening of the overall ephrinA gradient in the SC.

Conclusion

The analysis of conditional ephrinA5 KO mice has uncovered that repellent axon-axon interactions contribute to topographic mapping specificity in central SC. However, our analysis has re-emphasized that we are far from understanding how topographic mapping in the visual system is controlled, given, for example, the unexplained mapping defects of peripheral temporal or nasocentral axons in these mice.

EXPERIMENTAL PROCEDURES

Mice

The transgenic mice (Efna5$^{tm1a(EUCOMM)Wtsi}$) were generated by the IKMC and the EUCOMM project (http://www.sanger.ac.uk/mouseportal/search?query=efna5) using the KO-first strategy (Skarnes et al., 2011). A 38k base pair sequence of the entire *ephrinA5* gene with integrated targeting cassette and frt and loxP sites is available under http://www.knockoutmouse.org/targ_rep/alleles/1301/escell-clone-genbank-file.

Mice expressing ubiquitously Flp recombinase (http://www.jax.org) were obtained from Pete Scambler (ICH, UCL); en-1:cre mice and *R26*-stop-EYFP mice (http://www.jax.org) were obtained from Albert Basson (Dental Institute, KCL); and the rx:cre mice were obtained from Robert Hindges (KCL). The ephrinA5 single KO and the ephrinA2/ephrinA5 DKO were obtained from David Feldheim's lab.

Antibodies

Polyclonal anti-GFP was raised in goat (GeneTex); Alexa-488 anti-goat was raised in donkey (Invitrogen).

DiI Tracing

Anterograde tracing experiments were essentially performed as described by Rashid et al. (2005). Following fixation, retinae were processed as described by D. Sterratt and colleagues (Sterratt et al., 2013). All experiments described here were approved by and performed in accordance with relevant institutional guidelines and regulations (Ethical Review Committee of Kings College London).

Intensity Measurements

TZs and eTZs were defined as the area above 20% peak fluorescence intensity following background subtraction. Background intensity was defined as the intensity value of a representative DiI-negative spot away from any TZ, but in the same SC. For relative intensity calculations, the eTZ area was divided by the combined area of TZ and eTZ, such that relative intensity = area^{eTZ}/area$^{(eTZ+TZ)}$.

For t-axon injections (Figure 4), a faint eTZ was sometimes visible by eye, but its intensity was below the 20% detection threshold. In these instances, the relative intensity was calculated as 0% (En-cre, 4 out of 13; Rx-En-cre, 2 out of 8).

Topography Measurements

Topographic position along the rostrocaudal axis in the SC was measured from whole-mount images as described by Bevins et al. (2011). Retinal position of focal injections was determined using the Retistruct software package recently described by Sterratt and colleagues (Sterratt et al., 2013). The experimental analysis of both the in vivo and in vitro experiments was done "blind" to the experimental condition.

Growth Cone Collapse Analysis In Vitro

Strips from temporal and nasal parts of E7 or E8 chick retina (Walter et al., 1987) were plated on a laminin-coated substrate and arranged in parallel. The distance between the strips was chosen such that outgrowing temporal and nasal RGC axons came into contact within 24–36 hr. Strips were cut perpendicular to the temporonasal axis and thus contained either temporal or nasal RGCs.

For the time-lapse analysis, we used a Nikon Eclipse Ti-E inverted microscope and Cool SNAP HQ2 camera. The interaction between temporal and nasal axons was analyzed for 3–10 hr. Pictures were taken with a 10× lens every minute with the entire area between the two strips documented. For this, pictures were taken from overlapping areas and stitched together using NIS software. Routinely, an area of about 4 × 2 mm was recorded. For data analysis, the area between nasal and temporal strips was subdivided into 10–18 regions of interest using ImageJ, analyzed individually, and then pooled.

We only analyzed axons which could be clearly identified as single growing axons for > 30 min before contact with other axons. Only the first contact was counted for each axon. Furthermore, we only included axons in the analysis which clearly advanced prior to contact and which had a clearly visible growth cone.

The interactions were scored as follows: "0", no growth cone collapse (axon crosses another axon without growth cone collapse and no/very little change in growth speed) (representative Movie S1); "0.3", a short transient growth cone collapse after contact and/or a clear slowing down of growth speed, but eventual crossing of the other axon (Movie S2); "0.6", a full growth cone collapse after contact (Movie S3); "1", a full growth cone collapse with a strong retraction of the axon (Movie S4).

The recordings were analyzed by two individuals independently and blind to the identity of the class of axons analyzed.

Immunohistochemistry

Immunohistochemical analysis of frozen sections was performed using standard procedures. Nonspecific interactions were blocked with 1% BSA-TBST,

primary antibody solution was applied overnight, and secondary antibody solution was applied for 2 hr, all at room temperature.

RT-PCR

RNA was extracted from littermate pups on the day of birth using standard protocols. For retina, RNA was extracted from the whole retina of one eye. For SC, RNA was extracted from the central third of the SC from one side. RNA was then reverse transcribed and PCR performed to detect the relative abundance of ephrinA5 expression levels (ephrinA5 FW: TTT GAT GGG TAC AGT GCC TGC GAC; ephrinA5 Rev: AAG CAT CGC CAG GAG GAA CAG TAG) or β-actin (β-actin FW: GAT GAC GAT ATC GCT GCG CTG GTC G; β-actin Rev: GCC TGT GGT ACG ACC AGA GGC ATA CAG) using the following protocol: 94°C, 5 min, 30× (94°C, 1 min; 60°C, 1 min; 72°C, 1 min) followed by 72°C, 10 min.

Genotyping

Genomic DNA was extracted using the HotSHOT method (Truett et al., 2000), and genotyping reactions were performed for the presence of *ephrinA5* wild-type, KO-first, and floxed alleles as well as *rx*:*cre* and *en-1*:*cre* alleles.

Thermal cycles for all three PCR reactions were as follows: 94°C, 5 min, 30× (94°C, 1 min; 60°C, 1 min; 72°C, 1 min) followed by 72°C, 10 min.

The following primers were used: ephrinA5 FW, AGAATCCAGAGACTGCTG ACATCT; ephrinA5 Rev1, TGAGGCCAAGTTTGTTTCCTTGAA; ephrinA5 Rev2, AGGACATACTGAAGTGGGAATCAG; rx-cre FW, GTTGGGAGAATGCTCCG TAA; rx-cre Rev, GTATCCCACAATTCCTTGCG; en1-cre FW, TAAAGATATCT CACGTACTGACGGTG; en1-cre Rev, TCTCTGACCAGAGTCATCCTTAGC.

PCR product sizes were as follows: ephrinA5 wild-type, 450 bps; ephrinA5 floxed, 530 bps; ephrinA5 KO-first, 734 bps; rx:cre, 362 bps; en-1:cre, 300 bps.

mRNA In Situ Hybridization

These experiments were performed as previously described (Maiorano and Hindges, 2013). The probe for ephrinA5 corresponds to the sequence of exon2. For ephrinA2 and ephrinA3, probes from the Allen Brain Atlas were used (http://www.brain-map.org).

SUPPLEMENTAL INFORMATION

Supplemental Information includes three figures and four movies and can be found with this article online at http://dx.doi.org/10.1016/j.neuron.2014.09.023.

ACKNOWLEDGMENTS

We would like to thank Matthew Grubb, Robert Hindges, Sarah Guthrie, Phillip Gordon-Weeks (all KCL), and Franco Weth (KIT, Germany) for critically reading the manuscript. We would also like to thank the International Knockout Mouse Consortium (IKMC) and the European Conditional Mouse Mutagenesis (EUCOMM) project for providing KO-first ephrinA5 mutant mice, in particular Wolfgang Wurst, Joel Schick, and Susan Marschall; Pete Scambler (ICH, UCL) for the frt-deleter line; Albert Basson (Dental Institute, KCL) for en-1:cre and *R26*-stop-EYFP mice; Robert Hindges (KCL) for rx:cre mice; and D. Feldheim (UCSC) for ephrinA2 and ephrinA5 full KO mice. We would also like to thank John Harris and Jan Soetaert from the Nikon Imaging Centre at KCL for expert advice in establishing time-lapse experiments. This work was supported by a Wellcome Trust programme grant (D. Willshaw [Principle Investigator], I. Thompson [KCL], S. Eglen [Cambridge], and U.D.), a Wellcome Trust project grant to U.D., and a BBSRC grant to U.D.

Accepted: September 3, 2014
Published: October 23, 2014

REFERENCES

Ackman, J.B., Burbridge, T.J., and Crair, M.C. (2012). Retinal waves coordinate patterned activity throughout the developing visual system. Nature *490*, 219–225.

Basson, M.A., Echevarria, D., Ahn, C.P., Sudarov, A., Joyner, A.L., Mason, I.J., Martinez, S., and Martin, G.R. (2008). Specific regions within the embryonic midbrain and cerebellum require different levels of FGF signaling during development. Development *135*, 889–898.

Bevins, N., Lemke, G., and Reber, M. (2011). Genetic dissection of EphA receptor signaling dynamics during retinotopic mapping. J. Neurosci. *31*, 10302–10310.

Bonhoeffer, F., and Huf, J. (1980). Recognition of cell types by axonal growth cones in vitro. Nature *288*, 162–164.

Bonhoeffer, F., and Huf, J. (1985). Position-dependent properties of retinal axons and their growth cones. Nature *315*, 409–410.

Brown, A., Yates, P.A., Burrola, P., Ortuño, D., Vaidya, A., Jessell, T.M., Pfaff, S.L., O'Leary, D.D., and Lemke, G. (2000). Topographic mapping from the retina to the midbrain is controlled by relative but not absolute levels of EphA receptor signaling. Cell *102*, 77–88.

Brunet, I., Weinl, C., Piper, M., Trembleau, A., Volovitch, M., Harris, W., Prochiantz, A., and Holt, C. (2005). The transcription factor Engrailed-2 guides retinal axons. Nature *438*, 94–98.

Cai, Z., Feng, G.S., and Zhang, X. (2010). Temporal requirement of the protein tyrosine phosphatase Shp2 in establishing the neuronal fate in early retinal development. J. Neurosci. *30*, 4110–4119.

Carreres, M.I., Escalante, A., Murillo, B., Chauvin, G., Gaspar, P., Vegar, C., and Herrera, E. (2011). Transcription factor Foxd1 is required for the specification of the temporal retina in mammals. J. Neurosci. *31*, 5673–5681.

Carvalho, R.F., Beutler, M., Marler, K.J., Knöll, B., Becker-Barroso, E., Heintzmann, R., Ng, T., and Drescher, U. (2006). Silencing of EphA3 through a cis interaction with ephrinA5. Nat. Neurosci. *9*, 322–330.

Cheng, H.J., Nakamoto, M., Bergemann, A.D., and Flanagan, J.G. (1995). Complementary gradients in expression and binding of ELF-1 and Mek4 in development of the topographic retinotectal projection map. Cell *82*, 371–381.

Davy, A., and Soriano, P. (2005). Ephrin signaling in vivo: look both ways. Dev. Dyn. *232*, 1–10.

Dhande, O.S., Bhatt, S., Anishchenko, A., Elstrott, J., Iwasato, T., Swindell, E.C., Xu, H.P., Jamrich, M., Itohara, S., Feller, M.B., and Crair, M.C. (2012). Role of adenylate cyclase 1 in retinofugal map development. J. Comp. Neurol. *520*, 1562–1583.

Drescher, U., Kremoser, C., Handwerker, C., Löschinger, J., Noda, M., and Bonhoeffer, F. (1995). In vitro guidance of retinal ganglion cell axons by RAGS, a 25 kDa tectal protein related to ligands for Eph receptor tyrosine kinases. Cell *82*, 359–370.

Dütting, D., Handwerker, C., and Drescher, U. (1999). Topographic targeting and pathfinding errors of retinal axons following overexpression of ephrinA ligands on retinal ganglion cell axons. Dev. Biol. *216*, 297–311.

Feldheim, D.A., and O'Leary, D.D. (2010). Visual map development: bidirectional signaling, bifunctional guidance molecules, and competition. Cold Spring Harb. Perspect. Biol. *2*, a001768.

Feldheim, D.A., Vanderhaeghen, P., Hansen, M.J., Frisén, J., Lu, Q., Barbacid, M., and Flanagan, J.G. (1998). Topographic guidance labels in a sensory projection to the forebrain. Neuron *21*, 1303–1313.

Feldheim, D.A., Kim, Y.I., Bergemann, A.D., Frisén, J., Barbacid, M., and Flanagan, J.G. (2000). Genetic analysis of ephrin-A2 and ephrin-A5 shows their requirement in multiple aspects of retinocollicular mapping. Neuron *25*, 563–574.

Frisén, J., Yates, P.A., McLaughlin, T., Friedman, G.C., O'Leary, D.D.M., and Barbacid, M. (1998). Ephrin-A5 (AL-1/RAGS) is essential for proper retinal axon guidance and topographic mapping in the mammalian visual system. Neuron *20*, 235–243.

Gebhardt, C., Bastmeyer, M., and Weth, F. (2012). Balancing of ephrin/Eph forward and reverse signaling as the driving force of adaptive topographic mapping. Development *139*, 335–345.

Gosse, N.J., Nevin, L.M., and Baier, H. (2008). Retinotopic order in the absence of axon competition. Nature *452*, 892–895.

Hansen, M.J., Dallal, G.E., and Flanagan, J.G. (2004). Retinal axon response to ephrin-as shows a graded, concentration-dependent transition from growth promotion to inhibition. Neuron *42*, 717–730.

Honda, H. (2003). Competition between retinal ganglion axons for targets under the servomechanism model explains abnormal retinocollicular projection of Eph receptor-overexpressing or ephrin-lacking mice. J. Neurosci. *23*, 10368–10377.

Hornberger, M.R., Dütting, D., Ciossek, T., Yamada, T., Handwerker, C., Lang, S., Weth, F., Huf, J., Wessel, R., Logan, C., et al. (1999). Modulation of EphA receptor function by coexpressed ephrinA ligands on retinal ganglion cell axons. Neuron *22*, 731–742.

Huberman, A.D., Feller, M.B., and Chapman, B. (2008). Mechanisms underlying development of visual maps and receptive fields. Annu. Rev. Neurosci. *31*, 479–509.

Kao, T.J., and Kania, A. (2011). Ephrin-mediated cis-attenuation of Eph receptor signaling is essential for spinal motor axon guidance. Neuron *71*, 76–91.

Klein, R. (2009). Bidirectional modulation of synaptic functions by Eph/ephrin signaling. Nat. Neurosci. *12*, 15–20.

Lim, Y.S., McLaughlin, T., Sung, T.C., Santiago, A., Lee, K.F., and O'Leary, D.D. (2008). p75(NTR) mediates ephrin-A reverse signaling required for axon repulsion and mapping. Neuron *59*, 746–758.

Maiorano, N.A., and Hindges, R. (2013). Restricted perinatal retinal degeneration induces retina reshaping and correlated structural rearrangement of the retinotopic map. Nat. Commun. *4*, 1938.

Marcus, R.C., Gale, N.W., Morrison, M.E., Mason, C.A., and Yancopoulos, G.D. (1996). Eph family receptors and their ligands distribute in opposing gradients in the developing mouse retina. Dev. Biol. *180*, 786–789.

Marler, K.J., Poopalasundaram, S., Broom, E.R., Wentzel, C., and Drescher, U. (2010). Pro-neurotrophins secreted from retinal ganglion cell axons are necessary for ephrinA-p75NTR-mediated axon guidance. Neural Dev. *5*, 30.

Marquardt, T., Shirasaki, R., Ghosh, S., Andrews, S.E., Carter, N., Hunter, T., and Pfaff, S.L. (2005). Coexpressed EphA receptors and ephrin-A ligands mediate opposing actions on growth cone navigation from distinct membrane domains. Cell *121*, 127–139.

McLaughlin, T., and O'Leary, D.D. (2005). Molecular gradients and development of retinotopic maps. Annu. Rev. Neurosci. *28*, 327–355.

Pfeiffenberger, C., Yamada, J., and Feldheim, D.A. (2006). Ephrin-As and patterned retinal activity act together in the development of topographic maps in the primary visual system. J. Neurosci. *26*, 12873–12884.

Pinter, R., and Hindges, R. (2010). Perturbations of microRNA function in mouse dicer mutants produce retinal defects and lead to aberrant axon pathfinding at the optic chiasm. PLoS ONE *5*, e10021.

Raper, J.A., and Grunewald, E.B. (1990). Temporal retinal growth cones collapse on contact with nasal retinal axons. Exp. Neurol. *109*, 70–74.

Rashid, T., Upton, A.L., Blentic, A., Ciossek, T., Knöll, B., Thompson, I.D., and Drescher, U. (2005). Opposing gradients of ephrin-As and EphA7 in the superior colliculus are essential for topographic mapping in the mammalian visual system. Neuron *47*, 57–69.

Reber, M., Burrola, P., and Lemke, G. (2004). A relative signalling model for the formation of a topographic neural map. Nature *431*, 847–853.

Schmidt, J.T. (1978). Retinal fibers alter tectal positional markers during the expansion of the retinal projection in goldfish. J. Comp. Neurol. *177*, 279–295.

Skarnes, W.C., Rosen, B., West, A.P., Koutsourakis, M., Bushell, W., Iyer, V., Mujica, A.O., Thomas, M., Harrow, J., Cox, T., et al. (2011). A conditional knockout resource for the genome-wide study of mouse gene function. Nature *474*, 337–342.

Sperry, R.W. (1963). Chemoaffinity in the orderly growth of nerve fiber patterns and connections. Proc. Natl. Acad. Sci. USA *50*, 703–710.

Sterratt, D.C., Lyngholm, D., Willshaw, D.J., and Thompson, I.D. (2013). Standard anatomical and visual space for the mouse retina: computational reconstruction and transformation of flattened retinae with the Retistruct package. PLoS Comput. Biol. *9*, e1002921.

Suetterlin, P., Marler, K.M., and Drescher, U. (2012). Axonal ephrinA/EphA interactions, and the emergence of order in topographic projections. Semin. Cell Dev. Biol. *23*, 1–6.

Swindell, E.C., Bailey, T.J., Loosli, F., Liu, C., Amaya-Manzanares, F., Mahon, K.A., Wittbrodt, J., and Jamrich, M. (2006). Rx-Cre, a tool for inactivation of gene expression in the developing retina. Genesis *44*, 361–363.

Triplett, J.W., and Feldheim, D.A. (2012). Eph and ephrin signaling in the formation of topographic maps. Semin. Cell Dev. Biol. *23*, 7–15.

Truett, G.E., Heeger, P., Mynatt, R.L., Truett, A.A., Walker, J.A., and Warman, M.L. (2000). Preparation of PCR-quality mouse genomic DNA with hot sodium hydroxide and tris (HotSHOT). BioTechniques *29*, 52–54.

Walter, J., Henke-Fahle, S., and Bonhoeffer, F. (1987). Avoidance of posterior tectal membranes by temporal retinal axons. Development *101*, 909–913.

Willshaw, D.J., Sterratt, D.C., and Teriakidis, A. (2014). Analysis of local and global topographic order in mouse retinocollicular maps. J. Neurosci. *34*, 1791–1805.

Wizenmann, A., Brunet, I., Lam, J.S., Sonnier, L., Beurdeley, M., Zarbalis, K., Weisenhorn-Vogt, D., Weinl, C., Dwivedy, A., Joliot, A., et al. (2009). Extracellular Engrailed participates in the topographic guidance of retinal axons in vivo. Neuron *64*, 355–366.

Yates, P.A., Holub, A.D., McLaughlin, T., Sejnowski, T.J., and O'Leary, D.D. (2004). Computational modeling of retinotopic map development to define contributions of EphA-ephrinA gradients, axon-axon interactions, and patterned activity. J. Neurobiol. *59*, 95–113.

Yoo, S., Kim, Y., Noh, H., Lee, H., Park, E., and Park, S. (2011). Endocytosis of EphA receptors is essential for the proper development of the retinocollicular topographic map. EMBO J. *30*, 1593–1607.